Science Arts & Métiers (SAM)
is an open access repository that collects the work of Arts et Métiers Institute of Technology researchers and makes it freely available over the web where possible.

This is an author-deposited version published in: https://sam.ensam.eu
Handle ID: .http://hdl.handle.net/10985/10095

To cite this version :

M. SCHMITT, Rachele ALLENA, T. SCHOUMAN, S. FRASCA, J.M. COLLOMBET, X. HOLY, Philippe ROUCH - Diffusion model to describe osteogenesis within a porous titanium scaffold. - Computer Methods in Biomechanics and Biomedical Engineering - Vol. 9, p.1-9 - 2015

Any correspondence concerning this service should be sent to the repository Administrator : scienceouverte@ensam.eu

Diffusion model to describe osteogenesis within a porous titanium scaffold

M. Schmitt[a]*, R. Allena[a], T. Schouman[a,b], S. Frasca[c], J.M. Collombet[c], X. Holy[c] and P. Rouch[a]

[a]*Arts et Métiers ParisTech, LBM, 151 bd de l'hôpital, 75013 Paris, France;* [b]*Department of maxillofacial surgery, APHP – Pitie-Salpetriere University Hospital, University of Paris 6, 75013 Paris, France;* [c]*Institut de recherche biomédicale des armées, 91223 Brétigny sur Orge, France*

In this study, we develop a two-dimensional finite element model, which is derived from an animal experiment and allows simulating osteogenesis within a porous titanium scaffold implanted in ewe's hemi-mandible during 12 weeks. The cell activity is described through diffusion equations and regulated by the stress state of the structure. We compare our model to (i) histological observations and (ii) experimental data obtained from a mechanical test done on sacrificed animal. We show that our mechano-biological approach provides consistent numerical results and constitutes a useful tool to predict osteogenesis pattern.

Keywords: bone scaffold; osteogenesis; *in vivo* test; finite element method; mechanobiology

1. Introduction

Bone is a living tissue able to rebuild and restore its physical and geometrical properties when injured. Specifically, bone remodelling and bone ingrowth are two important biological phenomena that successively occur during fracture healing process, prosthesis osseointegration and distraction osteogenesis (Meyrueis and Cazenave 2004). Nevertheless, when a defect exceeds a critical size for spontaneous bone formation (Schmitz and Hollinger 1986), a structural support such as a porous implant (i.e. scaffold) is required to enhance bone ingrowth and to ensure the mechanical loads transmission.

During the last decades, many *in vivo* studies on rodents (i.e. rabbits or rats) have evaluated the osseointegration of porous implants (Karageorgiou and Kaplan 2005; Takemoto et al. 2005; St-Pierre et al. 2005; Otsuki et al. 2006; Lopez-Heredia et al. 2008). Nonetheless, besides the high cost of experimentations, osteogenesis is a long process with successive steps, which makes its experimental observation very difficult. Therefore, mathematical and numerical models have been proposed in the literature to better understand the complex process of osteogenesis and optimize the design of the scaffolds.

These models can be divided into two main categories: the multi-physics and the multi-scale models. The former consider the mechanoregulatory process that may take place during bone ingrowth and osteogenesis. Different theories emerged demonstrating that mechanics plays an important role on the cellular activity. Pauwels (1960) was the first to hypothesize that mechanical stresses and strains could determine the differentiation pathways of mesenchymal stem cells (MSCs). Specifically, he found that during bone fracture healing, bone formation only occurs once fracture stabilization is ensured by fibrous tissues. Carter et al. (1988) suggested that MSCs are more likely to become osteogenic if they are submitted to low shear strain and compressive hydrostatic stress. In Prendergast et al. (1997), the coupling between the fluid–solid velocity and the maximal shear strain is considered as a key factor for the regulation of cell differentiation. Such an approach has been widely used to predict tissue regeneration during fracture healing (Lacroix and Prendergast 2002; Isaksson et al. 2008), distraction osteogenesis (Isaksson et al. 2007) and also tissue ingrowth within scaffolds (Kelly and Prendergast 2006; Liu and Niebur 2008) or at bone–implant porous interface (Huiskes et al. 1997; Andreykiv et al. 2005; Andreykiv et al. 2008). Other mechanobiological models have been proposed using different techniques resulting in random walk models (Pérez and Prendergast 2007; Byrne et al. 2007), lattice-based models (Checa and Prendergast 2010; Sandino et al. 2010), biological model (Moreo et al. 2009) and voxel finite element (FE) models (Adachi et al. 2006; Sanz-Herrera et al. 2008, 2009).

The multi-scale models distinguish between two spatio-temporal scales at the tissue and at the pore-scaffold level. Among these works, we mention those from Prendergast et al. (1997), Kelly and Prendergast (2006) and Sanz-Herrera et al. (2008, 2009) in which the influence of both the cellular activity and the scaffold microstructure is considered. In addition, some homogenization approaches (Hollister et al. 2002, Taboas et al. 2003,

*Corresponding author. Email: mary.schmitt-8@etudiants.ensam.eu

Hutmacher et al. 2004) have been used to design and control the scaffold porosity and pores size.

Most of the previous works are defined by a large number of parameters, which are difficult to determine experimentally, and therefore the results are only qualitatively compared to the experimental observations. An alternative approach was proposed by Roshan-Ghias et al. (2011) according to which bone osteogenesis is regulated by a diffusion phenomenon and the few unknown variables of the model are identified through *in vivo* micro-computed tomography (micro-CT).

In the present paper, we introduce a two-dimensional (2D) FE model derived from a specific animal study. Our main goal is to propose a new numerical approach to describe osteogenesis within a titanium scaffold implanted in a ewe's hemi-mandible. The key feature of the model lays on the link between mechanics and biology, which is stronger than those proposed in previous works. In fact, the cellular activity (i.e. migration and proliferation) is defined through diffusion equations, which are coupled twice with the mechanical framework of the problem through (i) the principal stresses and (ii) the principal directions. At the end of the bone-remodelling process, which takes 12 weeks in our specific case (Den Boer et al. 1999), the numerical results are compared to the experimental ones in two different ways. First, we qualitatively correlate the cell density and colonization patterns to the histological data obtained on an implanted hemi-mandible. Secondly, we quantitatively assess the consistence of the same results by performing a cantilever bending simulation on the colonized hemi-mandible and comparing it to the corresponding experimental deflection.

2. Methods

2.1 Scaffold and experimental set up

In this present study, an 18-mm long titanium scaffold with a porosity of 53% was placed after resection of the non-toothed part of ewes' hemi-mandibles. To anchor the scaffold to the bone, 10 titanium screws were used (Figure 1(b)). The scaffold was designed and produced by OBL® using a selective laser melting (SLM) technique (Barbas et al. 2012).

Three ewes' hemi-mandibles were tested:

- a non-implanted (NI-0, Figure 1(a)) and an implanted (I-0, Figure 1(b)) hemi-mandibles coming from the same ewe sacrificed right after scaffold implantation ($t = 0$);
- an implanted (I-12, Figure 2(a)) hemi-mandible coming from a ewe sacrificed 12 weeks after scaffold implantation ($t = 12$ weeks).

Both ewes were approximately 2 years old. A cantilever bending test was performed on each hemi-mandible using a universal traction machine (INSTRON 5500-R).

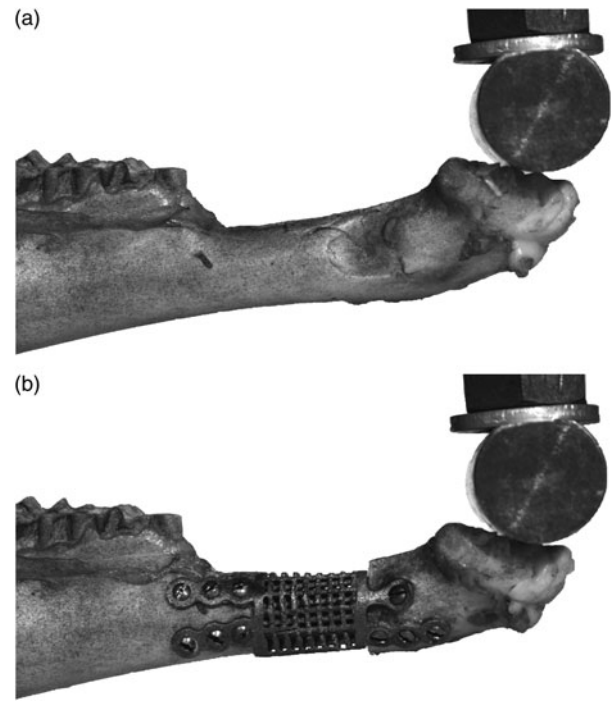

Figure 1. The NI-0 (a) and I-0 (b) hemi-mandible coming from the same ewe sacrificed right after scaffold implantation ($t = 0$). In (b), the 18-mm-long titanium scaffold placed after resection of the non-toothed part of the I-0 hemi-mandible and anchored to the bone with 10 titanium screws is noticeable.

Before the test, a black and white speckle pattern was painted on the hemi-mandible in order to perform digital images correlation (DIC). The proximal boundary of the hemi-mandible was embedded into polymethylmetacrylate (PMMA), while the distal boundary was submitted to a displacement of 2 mm/min, which was applied until failure through a cylinder load nose. The resultant force was measured using a load cell of 1 KN.

During the test, the hemi-mandible was kept wet to avoid the drying of the bone, which could have altered its mechanical properties (Evans and Lebow 1952; Blackburn et al. 1992). Finally, frontal images of the set-up were captured every 2 s using a digital camera.

2.2 Histological evaluation

After micro-CT, defect areas including a 5-mm edge of native bone at both the anterior and posterior margins were excised from the hemi-mandible I-12. The segments were fixed for at least 7 days in 10% phosphate-buffered formaldehyde solution.

Undecalcified segments were sectioned with a diamond saw (Secotom, Struers) along the antero-posterior direction thereafter dehydrated with methanol, and then embedded in methyl-methacrylate-based resin. The hardened specimen blocks were cut in the longitudinal

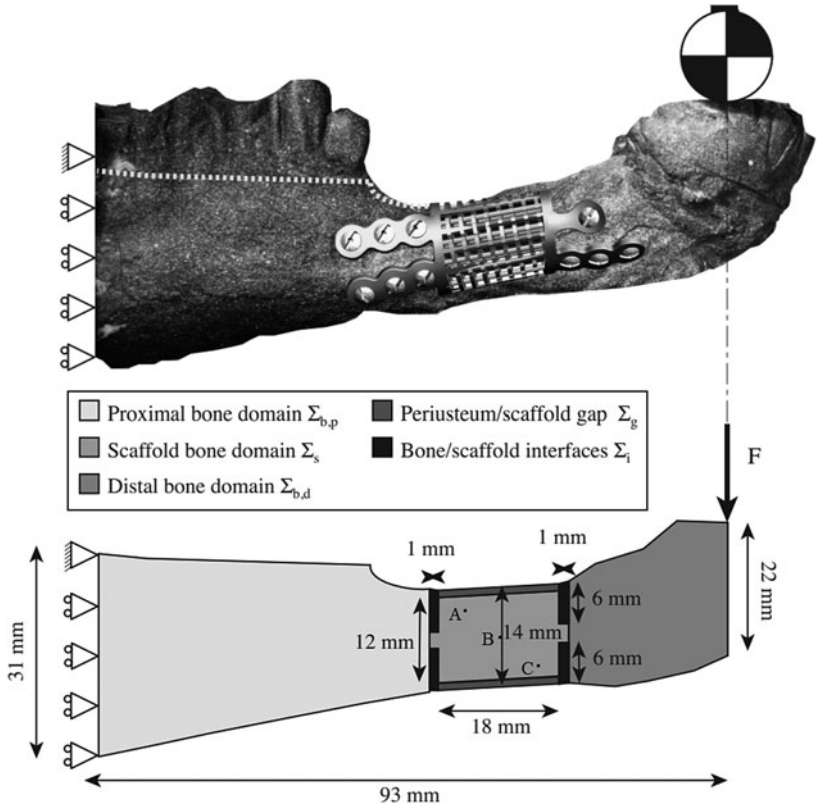

Figure 2. (a) The I-12 hemi-mandible. (b) The FE model geometry: dimensions, boundary conditions and subdomains of the implanted hemi-mandible. A, B and C indicate the three points used to evaluate c_m for the sensitivity analysis (see Appendix).

direction along the axis of the implant. Sections of interest were sawn off with the diamond saw, ground and finally polished up with a Buelher micro-grinding device to reach 100 μm thickness.

Finally, sections were stained with modified Masson–Goldner's trichrome dye to evaluate bone healing efficiency by histomorphometry and examined under a light microscopy (DMRB Leica, DXC930 Camera Sony).

2.3 Mechano-biological FE model

The mechano-biological framework of the FE model allows simulating the bone ingrowth within the titanium scaffold implanted in the hemi-mandible. Because the mandible is considered as a flat bone, here we only take into account intramembranous ossification, which, in contrast to endochondral ossification, does not require cartilaginous tissue.

The 2D geometry representing a sagittal view of the hemi-mandible (Figure 2(b)) has been obtained from the frontal digital images through DIC. The hemi-mandible is constituted by a proximal and a distal bone domains, $\Sigma_{b,p}$ and $\Sigma_{b,d}$, respectively. In addition, it includes a central domain composed of the scaffold Σ_s, which is placed between the two gaps, Σ_g, between the periosteum and the scaffold, and four interfaces Σ_{ij} (the subscript j indicates the interface number) between the scaffold and the bone. The domains Σ_s and Σ_{ij} have been represented through specific characteristic functions h_s and h_{ij}.

Here, we consider that each domain is made of an isotropic linear elastic material. For $\Sigma_{b,p}$ and $\Sigma_{b,d}$, homogenized Young's moduli ($E_{b,p}$ and $E_{b,d}$, respectively) have been deduced from the experimental deflection curve of the neutral axis of the hemi-mandible. For Σ_s, Σ_{ij} and Σ_g, we assume that, at the initial configuration, they are filled with a granular tissue, which will be gradually replaced by bone during the 12 weeks. Consequently, E_s, E_{ij} and E_g vary with respect to time and bone mineralization and are defined as follows:

$$E_s = \big(E_{s,0}\big(1 - \varnothing_{s,0}\big) + \varnothing_{s,0}\big(E_t\big(1 - c_m h_{\tau_m}\big) + E_b c_m h_{\tau_m}\big)\big)h_s, \tag{1}$$

$$E_{ij} = \big(E_t\big(1 - c_m h_{\tau_m}\big) + E_b c_m h_{\tau_m}\big)h_{ij}, \tag{2}$$

$$E_g = E_t\big(1 - c_m h_{\tau_m}\big) + E_b c_m h_{\tau_m}, \tag{3}$$

where $E_{s,0}$ is the initial Young's modulus of the scaffold, E_t and E_b are the Young's moduli of the granular tissue and the newly formed bone, respectively, $\varnothing_{s,0}$ is the scaffold initial porosity and c_m is the MSCs concentration, which is

defined as the fraction of MSCs inside the scaffold. h_{τ_m} is a characteristic function allowing to initiate the mineralization process. In fact, as the osteoblasts activity is not directly modelled, we assume that the mineralization starts after a maturation time τ_m of the MSCs of about 2 weeks (Malaval et al. 1999) and takes approximately 3 weeks to complete (Eriksen et al. 1986). Thus, the fraction of mineralized bone m_b inside the scaffold is defined as

$$m_b = c_m h_{\tau_m}. \tag{4}$$

We assume that both c_m and m_b are normalized and vary between 0 and 1.

During the simulation, the proximal boundary of the hemi-mandible is allowed to translate along the y-axis (except for the upper point which is completely blocked), while the distal boundary is submitted to a constant force to simulate the ewes' mastication (Thomason et al. 2001) (Figure 2(b)).

In the following, the diffusion equations used to describe the evolution of the MSCs concentration c_m within the different domains of the system are presented. Inside $\Sigma_{b,p}$ and $\Sigma_{b,d}$, we consider that c_m is constant with respect to time, while a Robin condition on $\partial\Sigma_{b,p}$ and $\partial\Sigma_{b,d}$ is applied to reproduce the cell proliferation outside the system. Thus, the diffusion equation reads

$$\frac{\partial c_m}{\partial t} = \operatorname{div}\left(\mathbf{D_{m,b}} \operatorname{grad} c_m\right) \quad \text{on } \Sigma_{b,p} \text{ and } \Sigma_{b,d}, \tag{5}$$

$$\begin{aligned} (\mathbf{D_{m,b}} \operatorname{grad} c_m, \mathbf{n}) &= -\gamma\left(c_{m,0} - c_m\right) \\ &\text{on } \partial\Sigma_{b,p} \text{ and } \partial\Sigma_{b,d}, \end{aligned} \tag{6}$$

where div and grad represent the divergence and the gradient, respectively, $(\mathbf{a},\mathbf{b})$ defines the scalar product between two vectors, γ is a constant, $c_{m,0}$ is the initial concentration of the MSCs inside the domains and $\mathbf{n}$ is the outward normal vector along the external boundaries. $\mathbf{D_{m,b}}$ is a tensor which couples the concentration c_m with the principal stresses and directions as follows:

$$\mathbf{D_{m,b}} = \alpha_b \mathbf{I} + \beta_b\left(\sqrt{|\sigma_I|}\varnothing_{\boldsymbol{\sigma_I}} \otimes \varnothing_{\boldsymbol{\sigma_I}} + \sqrt{|\sigma_{II}|}\varnothing_{\boldsymbol{\sigma_{II}}} \otimes \varnothing_{\boldsymbol{\sigma_{II}}}\right), \tag{7}$$

where α_b and β_b are specific constants, $\mathbf{I}$ is the identity matrix and $\varnothing_{\boldsymbol{\sigma_I}}$ and $\varnothing_{\boldsymbol{\sigma_{II}}}$ are the principal directions of the principal stresses σ_I and σ_{II}. $|\cdot|$ and $\otimes$ indicate the absolute value and the tensorial product, respectively.

The evolution of c_m within the scaffold is also defined by a diffusion equation as follows:

$$\frac{\partial c_m}{\partial t} = \operatorname{div}\left(\mathbf{D_{m,s}} \operatorname{grad} c_m\right) + P_m, \tag{8}$$

where the first and the second terms on the right-hand side describe the migration and the proliferation processes, respectively. As in Equation (6), $\mathbf{D_{m,s}}$ is coupled with the mechanics of the problem and reads

$$\mathbf{D_{m,s}} = \alpha_s \mathbf{I} + \beta_s\left(\sqrt{|\sigma_I|}\varnothing_{\boldsymbol{\sigma_I}} \otimes \varnothing_{\boldsymbol{\sigma_I}} + \sqrt{|\sigma_{II}|}\varnothing_{\boldsymbol{\sigma_{II}}} \otimes \varnothing_{\boldsymbol{\sigma_{II}}}\right), \tag{9}$$

where α_s and β_s are specific constants. The MSCs proliferation P_m is expressed as

$$P_m = P_{m,0}(1 - c_m)c_m, \tag{10}$$

with $P_{m,0}$ the MSCs production rate. MSCs migrate from the proximal and the distal bone domains but also from the periosteum. Thus, the previous diffusion equation is coupled with a Robin condition on the periosteum boundaries $\partial\Sigma_p$:

$$(\mathbf{D_{m,s}} \operatorname{grad} c_m, \mathbf{n}) = -\gamma(c_{m0} - c_m) \quad \text{on } \partial\Sigma_p. \tag{11}$$

3. Results

3.1 *Experimental results*

As mentioned in Section 2.1, a cantilever bending test was performed on three hemi-mandibles: NI-0, I-0 and I-12. The experimental deflection curves are represented in Figure 3.

First, it is possible to observe a clear difference between the two curves NI-0 and I-0. In fact, for NI-0 the curve is mostly straight, while for I-0 the curve presents two local changes in slope corresponding to the proximal and distal bone–scaffold interfaces, respectively.

Secondly, by comparing the curve of I-0 at $t = 0$ to the curve of I-12 at $t = 12$ weeks, it is possible to notice that the deflection is less important for the latter than for the former.

These outputs confirm that (i) the scaffold does not support the entire load and (ii) the cell colonization and mineralization do affect the global mechanical response of the system via the increase in the Young modulus inside the scaffold and at the interfaces of the scaffold with the proximal and distal bones.

3.2 *Numerical osteogenesis*

The numerical simulation has been run using the FE software COMSOL 3.5a. The main parameters associated with the constitutive behaviour of the system and the cellular activity are reported in Table 1.

In Figure 4, the results at the end of the process (i.e. 12 weeks) are represented. The MSCs concentration c_m varies between 0.3 and 1, respectively, at the centre and along the external boundaries of the scaffold (Figure 4(a)). More specifically, at points A, B and C (Figure 2(b)), c_m is equal to 0.61, 0.36 and 0.6, respectively. Because the

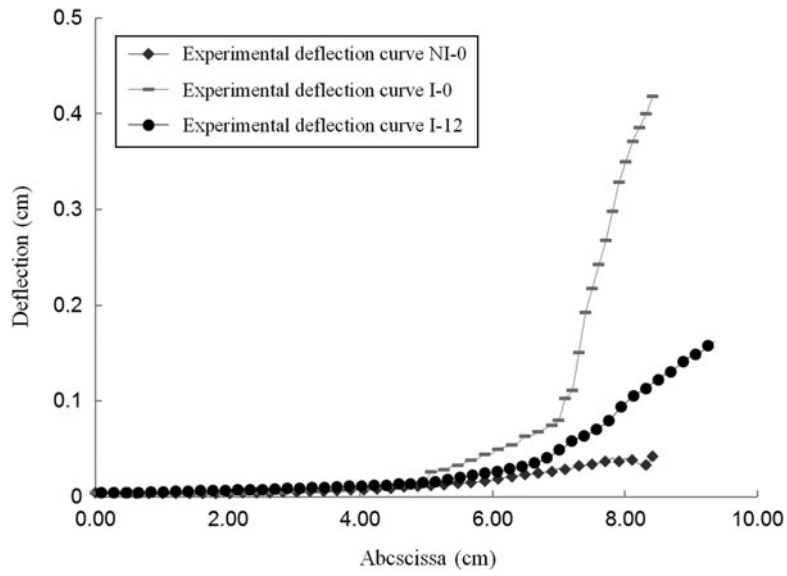

Figure 3. Experimental deflection curves of the neutral axis of NI-0 and I-0 at $t = 0$ and of I-12 at $t = 12$ weeks.

mineralization process starts after 2 weeks of maturation and takes approximately 3 weeks to complete (Section 2.3), we observe a complete cellular mineralization (i.e. equal to 1) at about 5 weeks after maturation (Figure 4(b)). We notice that the colonization and the mineralization patterns are very similar and occur from the outer boundaries towards the central region of the scaffold. In addition, the four interfaces Σ_{ij}, which were initially filled by a granular tissue, are now completely mineralized. Thus, according to Equation (1), the global stiffness of the scaffold is increased by the end of the simulation.

In Figure 5(a), a sagittal view of the middle section of the scaffold histological examination is reported. We distinguish between the mineralized bone (blue) and the fibrous tissue (purple), which are mostly distributed at the periphery and at the centre of the scaffold, respectively. The histological analysis provided a ratio bone volume (BV)/total volume (TV) equal to 62%. The direct comparison with our numerical results is not possible due to the fact that (i) the FE model is 2D and (ii) the scaffold pores are not physically modelled here. Nevertheless, thanks to the specific in-house Matlab software, we have been able to evaluate the ratio bone surface (BS)/total surface (TS) on Figure 5(a) and a value of 27% was obtained. For the FE model, we considered that bone is mineralized when m_b (Equation 4) is higher than 0.8. Then, the numerical value of BS/TS after 12 weeks is equal to 29% (Figure 5(b)). Therefore, we may conclude that our numerical results are qualitatively and quantitatively in agreement with the histological data.

Table 1. Model parameters.

Variable	Symbol	Value	Unit	Reference
Young's modulus of the proximal bone	$E_{b,p}$	6500	MPa	Deduced from DIC
Young's modulus of the distal bone	$E_{b,d}$	300	MPa	Deduced from DIC
Initial Young's modulus of the scaffold	$E_{s,0}$	60	GPa	Deduced from Barbas et al. (2012)
Young's modulus of granular tissue	E_t	0.2	MPa	Andreykiv et al. (2008)
Young's modulus of newly formed bone	E_b	200	MPa	Deduced from Nafei et al. (2000)
Initial porosity of the titanium scaffold	$\varnothing_{s,0}$	0.53		Barbas et al. (2012)
Robin constant	γ	$1e^{-7}$	m^2/s	
The initial concentration of the MSCs	$c_{m,0}$	0.98		
Diffusion constant in the bone domain	α_b	$1e^{-20}$	m^2/s	
Diffusion constant in the bone domain	β_b	$3e^{-13}$	m^2/s	
Diffusion constant in the scaffold domain	α_s	$1e^{-20}$	m^2/s	
Diffusion constant in the scaffold domain	β_s	$3e^{-15}$	m^2/s	
The MSCs production rate	$P_{m,0}$	$2e^{-9}$	s^{-1}	
MSCs maturation time	τ_m	14	days	Malaval et al. (1999)

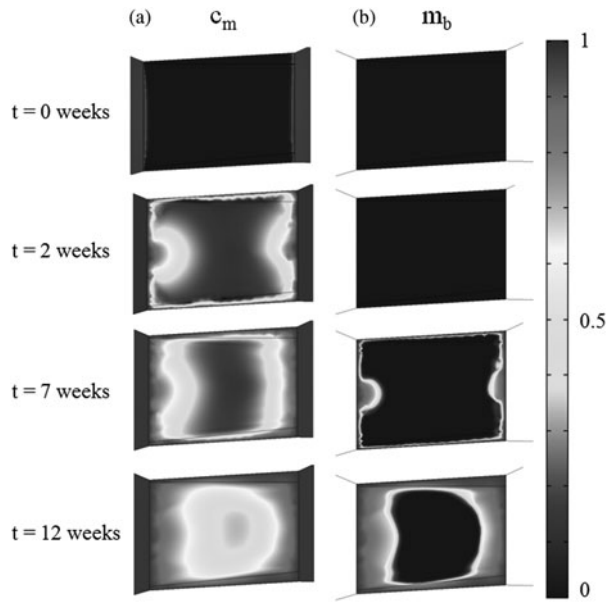

Figure 4. Time evolution of normalized MSCs concentration c_m (a) and of the fraction of mineralized bone m_b (b) within the scaffold predicted by the numerical simulation.

3.3 Comparison of the FE model to the experimental results

The cantilever bending test performed on the ewe's hemi-mandible 12 weeks after implantation (I-12) allows us to show the consistency of the FE model. In Figure 6, the experimental and the FE model deflection curves of the hemi-mandible's neutral axis at 12 weeks are represented. For both, the maximum deflection is reached at the distal boundary where the force is applied. Nevertheless, we obtained a maximal displacement of 1.62 mm for the former and of 1.46 mm for the latter. Furthermore, there are two local changes of the curve's slope which correspond to the proximal and distal bone–scaffold interfaces, respectively. Such a behaviour is mainly due to the low stiffness of the newly formed with respect to the proximal and distal bones.

Finally, in Figure 6, the FE model deflection curve of the hemi-mandible's neutral axis at the initial configuration is also represented. We notice that the maximum deflection after osteogenesis is about four times lower than the one obtained at the initial configuration (1.46 mm versus 5.65 mm, respectively). Such a difference is mainly due to the bone ingrowth within the scaffold and also at the bone–scaffold interfaces, which increase the global stiffness of the structure.

4. Discussion

In the literature, most of the models have not been validated (Andreykiv et al. 2005; Adachi et al. 2006; Andreykiv et al. 2008; Byrne et al. 2007: Liu and Niebur 2008) or validated through experimental tests on small animals (i.e. rabbits or rats) because their size and cost make the experimental protocol easier (Sanz-Herrera et al. 2008, 2009; Roshan-Ghias et al. 2011). Nevertheless, their bone properties are quite different than human's (Pearce et al. 2007). For instance, their characteristic time for bone remodelling is four times shorter (Sanz-Herrera et al. 2008). Therefore, our model is directly derived from an animal experiment done on bigger animals such as ewes. Indeed, the ovine model has been widely used in bone defect repair, distraction osteogenesis, osteoporosis and osteoarthritis research (Willie et al. 2004), and has been indicated as a valid model for the study of human bone remodelling and turnover (Den Boer et al. 1999; Pearce et al. 2007). The 2D FE model we have proposed allows simulating osteogenesis within a porous titanium scaffold implanted in a ewe's hemi-mandible for 12 weeks.

Cells migration and bone ingrowth within the scaffold are described through diffusion equations as previous authors did (Andreykiv et al. 2005; Kelly and Prendergast 2006; Liu and Niebur 2008; Andreykiv et al. 2008; Sanz-Herrera et al. 2008, 2009; Roshan-Ghias et al. 2011). Furthermore, the cells activity is directly coupled to the mechanics of the problem because MSCs migration follows the principal stresses and principal directions. Such a hypothesis results in bone ingrowth occurring from the external boundaries to the centre of the scaffold, which is in agreement with a previous study (Fujibayashi et al. 2003). The model has been correlated to the experimental

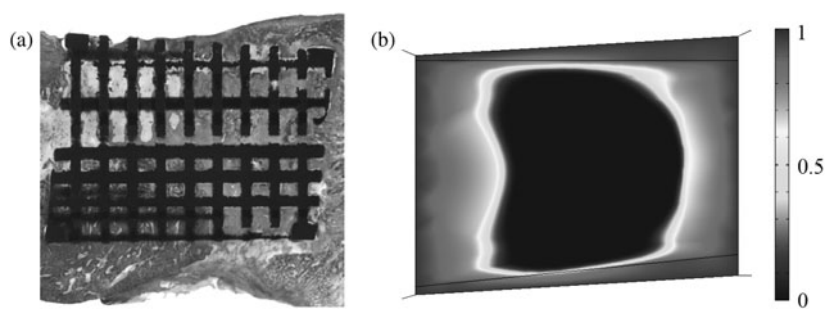

Figure 5. (a) Histological examination of the scaffold: stained middle section with modified Masson–Goldner's trichrome dye (mineralized bone in blue and fibrous tissues in purple). (b) Fraction of mineralized bone m_b at $t = 12$ weeks in the numerical model.

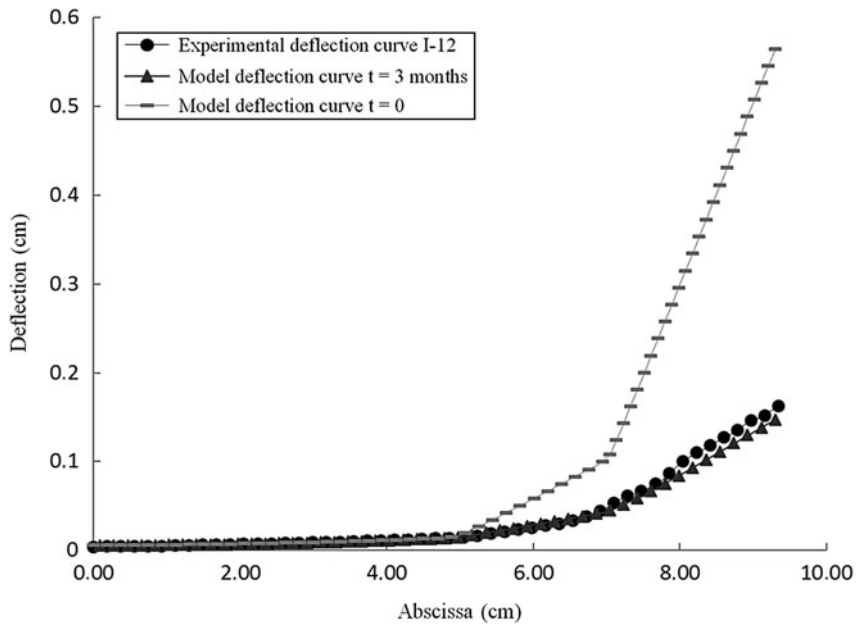

Figure 6. FE (at 0 and 12 weeks) and experimental (at 12 weeks) deflection curves of the neutral axis of the I-12 hemi-mandible.

data. For the former, a qualitative comparison between our numerical results and the histological observations has been done in terms of osteogenesis pattern. For the latter, the numerical and the experimental results obtained from a quasi-static bending test done on the 12 weeks ewe's hemi-mandible have been quantitatively compared. Although such a comparison has been done using the data from only one ewe and at a single time point, the FE model can still be considered as a useful and consistent tool to predict osteogenesis within the scaffold because the numerical results appear to be in agreement with the experimental ones.

Nevertheless, some assumptions have been done to develop the present work. First, a simplified 2D geometry has been employed to represent the implanted hemi-mandible. However, a 3D representation of the system may lead to a more realistic strain–stress distribution, which could influence the cells activity and thus the bone matrix distribution. Indeed, histological observations have pointed out that there might be more newly formed bone on the lingual region of the hemi-mandible than on the external region.

Second, the MSCs differentiation into either fibroblasts or osteoblasts is not regulated here by any biophysical stimulus derived from the interstitial flow and the shear strain (Prendergast et al. 1997) or the strain energy (Sanz-Herrera et al. 2008, 2009). Such stimulus would allow us to take into account all the cells types (i.e. fibroblasts and osteoblasts) involved in the intramembranous ossification.

Finally, we have not yet implemented the intrinsic properties of the implant such as its osteoconductive and osteoinductive characteristics.

Conflict of interest disclosure statement

No potential conflict of interest was reported by the authors.

Funding

This work has been funded by the Chaire BiomecAM, the Ministère de l'enseignement supérieur et de la recherche and OBL® Paris.

References

Adachi T, Osako Y, Tanaka M, Hojo M, Hollister SJ. 2006. Framework for optimal design of porous scaffold microstructure by computational simulation of bone regeneration. Biomaterials. 27(21):3964–3972.

Andreykiv A, Prendergast PJ, van Keulen F, Swieszkowski W, Rozing PM. 2005. Bone ingrowth simulation for a concept glenoid component design. J Biomech. 38(5):1023–1033.

Andreykiv A, van Keulen F, Prendergast PJ. 2008. Computational mechanobiology to study the effect of surface geometry on peri-implant tissue differentiation. J Biomech Eng. 130(5):051015.

Barbas A, Bonnet A-S, Lipinski P, Pesci R, Dubois G. 2012. Development and mechanical characterization of porous titanium bone substitutes. J Mech Behav Biomed. 9:34–44.

Blackburn J, Hodgskinson R, Currey JD, Mason JE. 1992. Mechanical properties of microcallus in human cancellous bone. J Orthop Res. 10(2):237–246.

Byrne DP, Lacroix D, Planell JA, Kelly DJ, Prendergast PJ. 2007. Simulation of tissue differentiation in a scaffold as a function of porosity, Young's modulus and dissolution rate: application of mechanobiological models in tissue engineering. Biomaterials. 28(36):5544–5554.

Carter DR, Blenman PR, Beaupré GS. 1988. Correlations between mechanical stress history and tissue differentiation in initial fracture healing. J Orthop Res. 6(5):736–748.

Checa S, Prendergast PJ. 2010. Effect of cell seeding and mechanical loading on vascularization and tissue formation inside a scaffold: A mechano-biological model using a lattice approach to simulate cell activity. J Biomech. 43(5): 961–968.

Den Boer FC, Patka P, Bakker FC, Wippermann BW, van Lingen A, Vink GQM, Boshuizen K, Haarman HJT. 1999. New segmental long bone defect model in sheep: Quantitative analysis of healing with dual energy X-ray absorptiometry. J Orthop Res. 17(5):654–660.

Eriksen EF, Mosekilde L, Melsen F. 1986. Trabecular bone remodeling and balance in primary hyperparathyroidism. Bone. 7(3):213–221.

Evans FG, Lebow M. 1952. The strength of human compact bone as revealed by engineering technics. AM J Surg. 83(3):326–331.

Fujibayashi S, Kim H-M, Neo M, Uchida M, Kokubo T, Nakamura T. 2003. Repair of segmental long bone defect in rabbit femur using bioactive titanium cylindrical mesh cage. Biomaterials. 24(20):3445–3451.

Hollister SJ, Maddox RD, Taboas JM. 2002. Optimal design and fabrication of scaffolds to mimic tissue properties and satisfy biological constraints. Biomaterials. 23(20):4095–4103.

Huiskes R, Driel WDV, Prendergast PJ, Søballe K. 1997. A biomechanical regulatory model for periprosthetic fibrous-tissue differentiation. J Mater Sci Mater Med. 8(12): 785–788.

Hutmacher DW, Sittinger M, Risbud MV. 2004. Scaffold-based tissue engineering: rationale for computer-aided design and solid free-form fabrication systems. Trends Biotechnol. 22(7):354–362.

Isaksson H, Comas O, van Donkelaar CC, Mediavilla J, Wilson W, Huiskes R, Ito K. 2007. Bone regeneration during distraction osteogenesis: Mechano-regulation by shear strain and fluid velocity. J Biomech. 40(9):2002–2011.

Isaksson H, van Donkelaar CC, Huiskes R, Ito K. 2008. A mechano-regulatory bone-healing model incorporating cell-phenotype specific activity. J Theor Biol. 252(2):230–246.

Karageorgiou V, Kaplan D. 2005. Porosity of 3D biomaterial scaffolds and osteogenesis. Biomaterials. 26(27): 5474–5491.

Kelly DJ, Prendergast PJ. 2006. Prediction of the optimal mechanical properties for a scaffold used in osteochondral defect repair. Tissue Eng. 12(9):2509–2519.

Lacroix D, Prendergast PJ. 2002. A mechano-regulation model for tissue differentiation during fracture healing: analysis of gap size and loading. J Biomech. 35(9):1163–1171.

Liu X, Niebur GL. 2008. Bone ingrowth into a porous coated implant predicted by a mechano-regulatory tissue differentiation algorithm. Biomech Model Mechanobiol. 7(4):335–344.

Lopez-Heredia MA, Sohier J, Gaillard C, Quillard S, Dorget M, Layrolle P. 2008. Rapid prototyped porous titanium coated with calcium phosphate as a scaffold for bone tissue engineering. Biomaterials. 29(17):2608–2615.

Malaval L, Liu F, Roche P, Aubin JE. 1999. Kinetics of osteoprogenitor proliferation and osteoblast differentiation in vitro. J Cell Biochem. 74(4):616–627.

Meyrueis J-P, Cazenave A. 2004. Consolidation des fractures [Fracture healing]. EMC - Rhumatologie-Orthopédie. 1(2):138–162. French.

Moreo P, García-Aznar JM, Doblaré M. 2009. Bone ingrowth on the surface of endosseous implants. Part 1: Mathematical model. J Theor Biol. 260(1):1–12.

Nafei A, Danielsen CC, Linde F, Hvid I. 2000. Properties of growing trabecular ovine bone. Part I: mechanical and physical properties. J Bone Joint Surg Br. 82(6):910–920.

Otsuki B, Takemoto M, Fujibayashi S, Neo M, Kokubo T, Nakamura T. 2006. Pore throat size and connectivity determine bone and tissue ingrowth into porous implants: three-dimensional micro-CT based structural analyses of porous bioactive titanium implants. Biomaterials. 27(35):5892–5900.

Pauwels F. 1960. Eine neue Theorie über den Einfluß mechanischer Reize auf die Differenzierung der Stützgewebe. Z Anat Entwickl Gesch. 121(6):478–515.

Pearce AI, Richards RG, Milz S, Schneider E, Pearce SG. 2007. Animal models for implant biomaterial research in bone: a review. Eur Cell Mater. 13:1–10.

Pérez MA, Prendergast PJ. 2007. Random-walk models of cell dispersal included in mechanobiological simulations of tissue differentiation. J Biomech. 40(10):2244–2253.

Prendergast PJ, Huiskes R, Søballe K. 1997. Biophysical stimuli on cells during tissue differentiation at implant interfaces. J Biomech. 30(6):539–548.

Roshan-Ghias A, Vogel A, Rakotomanana L, Pioletti DP. 2011. Prediction of spatio-temporal bone formation in scaffold by diffusion equation. Biomaterials. 32(29):7006–7012.

Sandino C, Checa S, Prendergast PJ, Lacroix D. 2010. Simulation of angiogenesis and cell differentiation in a CaP scaffold subjected to compressive strains using a lattice modeling approach. Biomaterials. 31(8):2446–2452.

Sanz-Herrera JA, García-Aznar JM, Doblaré M. 2008. Micro-macro numerical modelling of bone regeneration in tissue engineering. Comput Method Appl M. 197(33–40): 3092–3107.

Sanz-Herrera JA, García-Aznar JM, Doblaré M. 2009. On scaffold designing for bone regeneration: A computational multiscale approach. Acta Biomater. 5(1):219–229.

Schmitz JP, Hollinger JO. 1986. The critical size defect as an experimental model for craniomandibulofacial nonunions. Clin Orthop Relat Res. 205:299–308.

St-Pierre J-P, Gauthier M, Lefebvre L-P, Tabrizian M. 2005. Three-dimensional growth of differentiating MC3T3-E1 pre-osteoblasts on porous titanium scaffolds. Biomaterials. 26(35)–7328.

Taboas J, Maddox R, Krebsbach P, Hollister S. 2003. Indirect solid free form fabrication of local and global porous, biomimetic and composite 3D polymer-ceramic scaffolds. Biomaterials. 24(1):181–194.

Takemoto M, Fujibayashi S, Neo M, Suzuki J, Kokubo T, Nakamura T. 2005. Mechanical properties and osteoconductivity of porous bioactive titanium. Biomaterials. 26(30):6014–6023.

Thomason JJ, Grovum LE, Deswysen AG, Bignell WW. 2001. In vivo surface strain and stereology of the frontal and maxillary bones of sheep: implications for the structural design of the mammalian skull. Anat Rec. 264(4):325–338.

Willie BM, Bloebaum RD, Bireley WR, Bachus KN, Hofmann AA. 2004. Determining relevance of a weight-bearing ovine model for bone ingrowth assessment. J Biomed Mater Res A. 69(3):567–576.

Appendix

Sensitivity analysis

According to Table 1, the model presents 14 parameters. Among them, two have been determined from DIC ($E_{b,p}$ and $E_{b,d}$) and five have been found (E_t, $\varnothing_{s,0}$ and τ_m) or deduced ($E_{s,0}$ and E_b) from the literature. As for $c_{m,0}$, since we have assumed that both the proximal and the distal bone regions are completely fulfilled of MSCs throughout the simulation, a value of 0.98 has been fixed.

Therefore, to determine which parameters most influence the results and in particular the final value of the MSCs concentration c_m, a sensitivity analysis has been performed by letting vary of $\pm 10\%$ the remaining six parameters: γ, α_b, β_b, α_s, β_s and $P_{m,0}$. The value of c_m at $t = 12$ weeks has been evaluated at points A, B and C (Figure 1) and has been compared to the value obtained at the same points for the standard simulation (Section 3.2). The results are reported in Table 2.

As expected, the most influencing parameter is the diffusion constant in the scaffold domain β_s. In fact, as β_s increases or decreases, c_m increases (between 3.9% and 10%) and decreases (between 6% and 12%), respectively. However, when γ, α_b, α_s, β_b and $P_{m,0}$ change, the final value of c_m only undergoes a variation between 0.23% and 1.1%.

Table 2. Numerical results for the sensitivity analysis.

			Deviation of c_m with respect to the values in Section 3.2		
Constant	Variation (%)	Value	Point A (%)	Point B (%)	Point C (%)
γ	+10	$1.1e^{-7}$ m^2/s	−1.0	−0.77	+0.52
	−10	$0.9e^{-7}$ m^2/s	−1.1	−0.83	+0.23
α_b	+10	$1.1e^{-20}$ m^2/s	−0.83	−0.71	+0.44
	−10	$0.9e^{-20}$ m^2/s	−0.89	−0.74	+0.51
β_b	+10	$3.3e^{-13}$ m^2/s	−0.77	−0.56	+0.55
	−10	$2.7e^{-13}m^2/s$	−0.89	−0.78	+0.33
α_s	+10	$1.1e^{-20}$ m^2/s	−1.0	−0.83	+0.44
	−10	$0.9e^{-20}$ m^2/s	−0.69	−0.64	+0.49
β_s	+10	$3.3e^{-15}$ m^2/s	+3.9	+10	+6.0
	−10	$2.7e^{-15}$ m^2/s	−6.3	−12	−6.0
$P_{m,0}$	+10	$2.2e^{-9}$ s^{-1}	−0.78	−0.53	+0.45
	−10	1.8^{-9} s^{-1}	−0.85	−0.76	+0.56

Note: The value of c_m at $t = 12$ weeks has been evaluated at points A, B and C (Figure 1) and the deviations with respect to the reference values (Section 3.2) are reported.